

Accretion Properties of A Sample of Hard X-ray ($< 60\text{keV}$) Selected Seyfert 1 Galaxies

J. Wang¹ Y. F. Mao¹ and J. Y. Wei¹

*National Astronomical Observatories, Chinese Academy of Science, 20A Datun Road,
Chaoyang District, Beijing, China*

wj@bao.ac.cn

ABSTRACT

We examine the accretion properties in a sample of 42 hard (3-60keV) X-ray selected nearby broad-line AGNs. The energy range in the sample is harder than that usually used in the similar previous studies. These AGNs are mainly compiled from the RXTE All Sky Survey (XSS), and complemented by the released *INTEGRAL* AGN catalog. The black hole masses, bolometric luminosities of AGN, and Eddington ratios are derived from their optical spectra in terms of the broad $H\beta$ emission line. The tight correlation between the hard X-ray (3-20keV) and bolometric/line luminosity is well identified in our sample. Also identified is a strong inverse Baldwin relationship of the $H\beta$ emission line. In addition, all these hard X-ray AGNs are biased toward luminous objects with high Eddington ratio (mostly between 0.01 to 0.1) and low column density ($< 10^{22} \text{ cm}^{-2}$), which is most likely due to the selection effect of the surveys. The hard X-ray luminosity is consequently found to be strongly correlated with the black hole mass. We believe the sample completeness will be improved in the next few years by the ongoing *Swift* and *INTEGRAL* missions, and by the next advanced missions, such as NuSTAR, Simbol-X, and NeXT. Finally, the correlation between R_{Fe} (=optical Fe II/ $H\beta$) and disk temperature as assessed by $T \propto (L/L_{\text{Edd}})M_{\text{BH}}^{-1}$ leads us to suggest that the strength of the Fe II emission is mainly determined by the shape of the ionizing spectrum.

Subject headings: galaxies: Seyferts — X-rays: galaxies — quasars: emission lines

1. Introduction

It is now generally believed that the power of Active Galactic Nuclei (AGNs) is extracted through the accretion of gas onto a central supermassive black hole (SMBH). Such energy mechanism means that AGNs are characterized by their strong hard X-ray emission ($h\nu > 2\text{keV}$), which is widely used as direct evidence suggesting the existence of a nuclear accretion activity ($L_{2-8\text{keV}} > 10^{42} \text{ ergs s}^{-1}$, e.g., Silverman et al. 2005; Brusa et al. 2007; Hasinger et al. 2005). The commonly accepted model is that the hard X-ray emission from AGNs is primarily produced by the inverse Compton scattering of the UV/soft X-ray photons emitted from the accretion disk (e.g, Zdziarski et al. 1995, 2000; Haardt & Maraschi 1991; Kawaguchi et al. 2001). The absorption-corrected X-ray photon spectra within the energy band 2-10keV could be best described as a cut-off powerlaw with index $\Gamma \sim 1.9$ (e.g., Zdziarski et al. 1995; Reeves & Turner 2000; Piconcelli et al. 2005; Dadina 2008; Panessa et al. 2008). The synthesis spectra become flat beyond 10keV because of the Compton reflection caused by the ionized surface of the accretion disk (e.g., George & Fabian 1991).

Because the hard X-ray emission from central engine can penetrate the obscuration material much more easily than lower energy emission, it possesses particular importance in testing the traditional unified model (Antonucci 1993) in Seyfert 2 galaxies (e.g., Moran et al. 2002; Cardamone et al. 2007). The studies of the *Chandra* and *XMM-Newton* observatories showed that the cosmic X-ray background (CXRB) at 2-30keV might be contributed by many unknown obscured AGNs which are predicted by the CXRB models (e.g., Comastri et al. 1995; De Luca & Molendi 2004; Worsley et al. 2005; Gilli et al. 2007; Severgnini et al. 2003; Levenson et al. 2006). Taking into account of the issue of co-evolution of AGN and bulge of its host galaxy (e.g., Heckman et al. 2004; Kauffmann et al. 2003; Wang et al. 2006; Wang & Wei 2008 and references therein), the hard X-ray emission from AGNs is also an important tool in detecting and separating AGN's contribution from circumnuclear star formation activity. The X-ray luminosities of known most X-ray luminous starforming and elliptical galaxies are not higher than $L_X = 10^{42} \text{ erg s}^{-1}$ (Zezas et al. 2003; Lira et al. 2002a, 2002b; O'Sullivan et al. 2001).

Heckman et al. (2005) identified a very tight correlation between the hard X-ray (3-20keV) and [O III] luminosities in a sample of hard X-ray selected AGNs when they performed a comparison between the hard X-ray selected and [O III] emission-line selected AGNs. In 2-10keV bandpass, similar correlations were identified in the Palomar optically selected AGNs by Panessa et al. (2006). On the contrary, a very weak $L_{[\text{O III}]}-L_X$ correlation was identified in the AGNs selected by their bright [O III] emission lines (Heckman et al. 2005). The result suggests that many AGNs might be missed in the hard X-ray survey. Moreover, Netzer et al. (2006) claimed that the $L_{[\text{O III}]} / L_X$ ratio depends on the X-ray luminosity.

The questions are therefore naturally raised: why is the $L_{[\text{OIII}]}-L_X$ correlation broken in some kind of AGNs? which parameters (or what are the physical reasons that) determine the correlation? Are the hard X-ray selected AGNs particular in some parameters? Both black hole mass (M_{BH}) and Eddington ratio (L/L_{Edd}) are two key parameters determining the observed properties of AGNs. In addition, with the development of the technology in hard X-ray detection, a major advance in studying AGN hard X-ray emission will be achieved in the next a few years due to the launch of new missions with enhanced hard X-ray capability (in sensitivity and imaging), such as NuSTAR, Simbol-X, and NeXT (e.g., Takahashi et al. 2008; Ferrando et al. 2003). The study on the existent surveys certainly prepares the ground for the future surveys.

In this paper, we examine the optical spectral properties of a sample of 42 hard X-ray selected broad-line AGNs, which allows us to investigate the properties of M_{BH} and L/L_{Edd} in these hard X-ray AGNs. The sample is mainly compiled from the AGN catalog of the RXTE 3-20keV All Sky Survey (XSS, Sazonov & Revnivtsev 2004), and complemented by the AGN catalog released by the *INTEGRAL* all-sky hard X-ray survey (Bassani et al. 2006a and references therein). Note that the energy range used in this work is extended to the Compton reflection region, and is harder than the range (i.e., 0.5-10 keV) usually used in the similar previous studies. The paper is organized as follows. Section 2 and 3 shows the sample selection and spectroscopic observations, respectively. The data reduction is described in the next section. Section 5 presents the results and discussions. The cosmology with $h_0 = 0.7$, $\Omega_M = 0.3$, and $\Omega_\Lambda = 0.7$ (Bennett et al. 2003) is adopted in our calculations throughout the paper.

2. The Sample

Our sample is mainly compiled from the RXTE 3-20keV All-Sky Survey (XSS, Revnivtsev et al. 2004). Sazonov & Revnivtsev (2004, hereafter SR04) identified 95 nearby AGNs with $z_{\text{median}} \sim 0.035$ detected in XSS. The survey covers about 90% of the sky at $|b| > 10^\circ$. The sensitivity of the survey in the energy band 3-20 keV is better than $2.5 \times 10^{-11} \text{ergs s}^{-1} \text{cm}^{-2}$. SR04 therefore provides a nearly complete sample for bright hard X-ray selected AGNs, although the sample is still biased against sources with absorption column $N_{\text{H}} \geq 10^{23} \text{cm}^{-2}$. The IBIS telescope (Ubertini et al. 2003) onboard the *INTEGRAL* observatory (Winkler et al. 2003) provides a better capability for heavily obscured objects because of its good sensitivity beyond 20 keV. After about three years *INTEGRAL* observation, their all-sky survey project allows Bassani et al. (2006a) to identify 62 AGNs in the energy bandpass 20-100keV above a flux of $1.5 \times 10^{-11} \text{ergs s}^{-1} \text{cm}^{-2}$ by analyzing 11,300

INTEGRAL points (see also in Bassani et al. 2006b; Bird et al. 2006; Beckmann et al. 2006).

Both catalogs are then combined to enlarge our sample content, and to attempt to alleviate the bias against the obscuration. We further limit the objects to the broad-line AGNs according to the identification provided by previous optical spectroscopy. The BAT instrument (Barthelmy et al. 2005) onboard the *Swift* satellite (Gehrels et al. 2004) provides an all-sky hard X-ray survey with a sensitivity down to a few $\times 10^{-11}$ ergs s $^{-1}$ cm $^{-2}$ in higher energy band 14-195 keV. Markwardt et al. (2005) identified 44 previous known AGNs in the *Swift* survey. However, considering the spectroscopic observation condition (see below), only three objects are not listed in our sample. It is worthy noting that the ongoing *Swift*/BAT and *INTEGRAL* survey could provide a larger sample of ~ 100 hard X-ray selected AGNs at the end of our program (i.e., Krivonos et al. 2006; Sazonov et al. 2007; Tueller et al. 2008). We will perform a subsequent spectroscopic study on these AGNs in the next work.

Figure 1 shows the column density (N_{H}) distribution for our sample. N_{H} is compiled from SR04, and from Sazonov et al. (2007) for the objects detected by *INTEGRAL* only. Briefly, these authors determined N_{H} by fitting the available spectra from different X-ray instruments by an absorbed powerlaw. Values of N_{H} less than 10^{22} cm $^{-2}$ were ignored in the fitting of SR04 and Sazonov et al. (2007). As shown in the figure, the current sample is still strongly biased against AGNs with large column density.

3. Spectroscopic Observations

Both because of the constraint of the observatory site and because of the instrumental capability, the spectroscopic observations are only carried out for the bright ($m_v < 16.5$ mag) objects located in the northern sky with declination $\delta > -20^\circ$. In total, there are 53 objects fulfilling the selection criterion. Six of these objects are not observed because of the poor weather conditions. Among the remaining objects, five objects (i.e., XSSJ 02151-0033, XSS J11570+5514, XSS J22363-1230, NGC 788, IGR J21247+5058) are excluded in subsequent spectral modeling because of the weakness or absence of broad H α and/or H β emission lines¹

¹Our spectroscopic observations show that three objects, i.e., XSS J02151-0033, XSS J11570+5514, and XSS J22363-1230, could be further classified as Seyfert 1.9-like galaxies without broad components of Balmer emission lines except a broad H α emission. In addition, the continuum is dominated by the contribution from starlight of host galaxy rather than AGN in XSS J02151-0033 and XSS J11570+5514, which precludes the measurements of the Fe II complex. We include NGC 788 in our observation program because multi-classification is shown in the NED (see also in Beckmann et al. 2006). Our spectrum indicates a Seyfert 2

The total 42 high (or intermediate high) quality optical spectra were obtained by using the National Astronomical Observatories, Chinese Academy of Science (NAOC), 2.16m telescope in Xinglong observatory during several observing runs carried out from November 2005 to Mar 2008. The spectra were taken by the OMR spectrograph equipped with a back-illuminated SPEC10 1340×400 CCD as detector. A grating of 300g mm⁻¹ and a slit of 2.0" oriented in south-north direction were used in our observations. This setup results in a final spectral resolution $\sim 9\text{\AA}$ as measured from both comparison spectra and night sky emission lines. The blazed wavelength was fixed to be 6000Å, which provides a wavelength coverage of 3800-8300Å in observer frame. This attempt covers both H α and H β region in most spectra because of their small redshifts. Each object was observed successively twice. The two exposures were combined prior to extraction to enhance the S/N ratio and eliminate the contamination of cosmic-rays easily. The exposure time for each frame is generally between 900 and 3600 seconds depending on the brightness of the object. The wavelength calibration associated with each object was carried out by the helium-neon-argon comparison arcs taken between the two successive frames. The arcs were obtained at the position being nearly identical to that of the specified object. Two or three Kitt Peak National Observatory (KPNO) standard stars (Massey et al. 1988) were observed per night for both flux calibration and removal of the atmospheric absorption features. All the objects were observed as close to meridian as possible. Table 1 shows the log of observations of the 42 objects listed in our sample.

4. Data Reduction and Emission Line Measurements

The standard procedures using the IRAF package ² are adopted by us to reduce the unprocessed frames. The CCD reductions include bias subtraction, flat-field correction, and cosmic-rays removal before the extraction of signal. One-dimensional sky-subtracted spectra are then wavelength and flux calibrated. The uncertainties of the wavelength and flux calibrations are no more than 1Å and 20%, respectively. The Galactic extinctions

nucleus in the object. In fact, the object is classified as a Seyfert 2 galaxy with polarized broad emission lines in the catalogue of quasars and active nuclei (Veron-Cetty & Veron 2006). Our spectrum taken in Dec 20, 2006 shows that the spectrum of IGR J21247+5058 is dominated by a typical late type star, which is consistent with Masetti et al. (2004). By identifying the broad emission bump around 6700Å as H α , these author argued that the background AGN is aligned with a F- or early G-type star by chance.

²IRAF is distributed by the National Optical Astronomical Observatories, which is operated by the Association of Universities for Research in Astronomy, Inc., under cooperative agreement with the National Science Foundation.

are corrected by the color excess, the parameter $E(B - V)$ taken from the NASA/IAPC Extragalactic Database (NED), assuming an $R_V = 3.1$ extinction law of Milk Way (Cardelli et al. 1989). The spectra are then transformed to the rest frame, along with a k -correction, according to the narrow peak of $H\beta$.

4.1. Fe II subtractions

In order to determine the strength of the optical Fe II complex and to reliably profile the emission lines in $H\beta$ region, the Fe II complex should be modeled and then removed from each spectrum at first. We simply adopt the empirical template of the Fe II complex introduced in Boroson & Green (1992, hereafter BG92). For each object, the template is first broadened to the FWHM of the $H\beta$ broad component by convolving with a Gaussian profile (BG92). The broadened template and a broken powerlaw are combined to model the continuum by a χ^2 minimization for individual object. The minimization is performed over the rest frame wavelength range from 4300 to 7000Å, except for the regions around the strong emission lines (i.e., $H\alpha + [N II]$, $[S II]$, $H\beta$, $H\gamma$, $[O III]$, He II). The fittings are illustrated in the left column of Figure 2 for three typical cases. The flux of the Fe II complex is integrated between the rest wavelength 4434 and 4686Å. The Fe II complex is not measured in XSS J11067+7234 because its continuum is dominated by the starlight from the host galaxy.

4.2. Emission lines measurements

After removing the Fe II blends and continuum, the isolated AGN emission lines at $H\beta$ region are modeled by the SPECFIT task (Kriss 1994) in IRAF package. In each object, each of the $[O III]\lambda\lambda 4959, 5007$ doublet is modeled by a single Gaussian component. The flux ratio of the doublet is fixed to be 3 (e.g., Dimitrijevic et al. 2007). In principle, each $H\beta$ profile is modeled by a set of two Gaussian components: a narrow and a broad Gaussian component (denoted as $H\beta_n$ and $H\beta_b$, respectively). The profile modelings are illustrated for the three cases in the right column in Figure 2. The deblendings of the $H\beta$ emission line are, however, difficult in 15 objects because no obvious transition between the narrow and broad components is observed. In these 15 cases, the reported $H\beta_b$ measurements include both components, and the contribution of $H\beta_n$ is usually expected to be less than 3% for typical broad-line AGNs as suggested by BG92.

The described modeling works very well in most objects, except in three ones. In XSS J22539-1735, a very broad $H\beta$ component (FWHM $\sim 10,000$ km s $^{-1}$) is required to

properly reproduce the observed profile. Such component has been reported in $H\beta$ and highly ionized emission lines in previous studies (e.g., Sulentic et al. 2000b; Wang et al. 2005; Veron-Cetty et al. 2007; Marziani et al. 2003; Mullaney & Ward 2008; Hu et al. 2008). A double peaked and a boxy $H\beta$ profile is observed in XSS J18408+7947 and XSS J23073+0447, respectively. In all of the three cases, each $H\beta$ line is modeled by three Gaussian components, i.e., a narrow and two broad components. The modeled narrow component is then subtracted from the observed spectrum to derive a residual profile which is then used to measure FWHM and integrated flux.

5. Results and Discussion

Table 2 lists the following items measured from the spectra. Column (2) and (3) lists the equivalent widths (EWs) of $H\beta_n$ and $H\beta_b$, respectively. All the EWs refer to the continuum level determined from the continuum fitting at the position of wavelength $\lambda 4861$. The line ratio RFe ($=\text{Fe II}/H\beta_b$) is shown in column (4). Column (5) lists the luminosity of the $H\beta$ broad component, and Column (6) the FWHM of the broad $H\beta$ in units of km s^{-1} . All quoted widths are not corrected for the intrinsic resolution, since the widths are much broader than the resolution. Column (7) shows the luminosity of the [O III] emission line. Both [O III] and $H\beta_b$ luminosities are calculated from the cosmology-corrected luminosity distance ³ given by NED. The next two columns show the absorption-corrected hard X-ray luminosities in the bandpass 3-20 keV (XSS) and in 17-60 keV (*INTEGRAL*).

Six out of the 42 AGNs are detected by *INTEGRAL* only. In order to estimate their X-ray luminosities in the bandpass 3-20 keV from the luminosities in 17-60 keV, a transformation is derived in terms of the 18 objects detected by both surveys. The left panel of Figure 3 shows the relationship between the two sets of luminosity. A unweighted fitting yields a relationship $\log L_{17-60\text{keV}} = 1.03 \log L_{3-20\text{keV}} - 1.39$ with a standard deviation of 0.25. After transform the luminosities in the bandpass 17-60 keV to 3-20 keV for the six objects, the strong correlation between the [O III] and 3-20 keV luminosity is shown in the right panel of Figure 3 for the total 42 objects. The correlation is highly consistent with that derived in Heckman et al. (2005), which firmly demonstrates the accuracy of our observations and calibrations.

³Because the objects listed in our sample are generally very nearby, the radial velocity is corrected by a redshift of 0.017877 to the reference frame defined by the 3K Microwave Background Radiation.

5.1. Hard X-ray vs. bolometric luminosity

The detection of hard X-ray emission from a nucleus is regarded as strong evidence of accretion activity occurring around the central SMBH. The correlations between X-ray luminosity and luminosities of optical emission lines (e.g., $H\alpha$, $H\beta$, [O III]) have been extensively established in the previous studies (e.g., Elvis et al. 1984; Ward et al. 1988; Mulchaey et al. 1994; Heckman et al. 2005; Panessa et al. 2006). However, the correlations seem to depend on sample selection (Heckman et al. 2005) and on X-ray luminosity itself (Netzer et al. 2006). In this paper, we estimate the luminosity of AGN at rest wavelength 5100Å from the $H\beta_b$ component according to the calibration given by Greene & Ho (2005):

$$L_{5100} = 7.31 \times 10^{43} \left(\frac{L_{H\beta}}{10^{42} \text{ erg s}^{-1}} \right)^{0.883} \text{ ergs s}^{-1} \quad (1)$$

The bolometric luminosity is then derived by adopting the usually used bolometric correction $L_{\text{bol}} \approx 9\lambda L_{\lambda}(5100\text{\AA})$ (e.g., Kaspi et al. 2000). The significant correlation between L_{bol} and $L_{3-20\text{keV}}$ is shown in the left panel in Figure 4. A unweighted least square fitting gives a relationship:

$$\log L_X = (0.91 \pm 0.06) \log L_{\text{bol}} + (3.04 \pm 2.78) \quad (2)$$

or $L_{\text{bol}}/L_X \sim 10$ for simplification. The correlation strongly indicates a close link between the hard X-ray emission and ionizing radiation emitted from the accretion disk. Note that the bolometric luminosity spans four orders of magnitude, down to $L_{\text{bol}} \sim 10^{43} \text{ ergs s}^{-1}$, which is close to the formal definition of low luminous AGNs (i.e., $L_{\text{bol}} < 10^{43} \text{ ergs s}^{-1}$, Ho 2003). These faint galaxies generally radiate at low state with Eddington ratio marginally exceeds 0.01.

5.2. Black Hole Mass and Eddington Ratio

It is now generally believed that black hole mass (M_{BH}) and specific accretion rate (L/L_{Edd}) are two basic parameters determining the properties of AGNs. The role of L/L_{Edd} in driving the Eigenvector I (EI) space ⁴ has been extensively investigated in numerous previous studies (e.g., Boroson 2002; Sulentic et al. 2006; Xu et al. 2003; Grupe 2004;

⁴ The EI space is one of the key properties of AGN phenomena. It was first established by BG92 who analyzed the optical spectra of 87 bright PG quasars. In addition to the anti-correlation between the intensity of Fe II and [O III], the EI space has been subsequently extended to ultraviolet and soft X-ray bands (i.e., FWHM(C IV) and Γ_s , e.g., Wang et al. 1996; Xu et al. 2003; Grupe 2004; Sulentic et al. 2007; see Sulentic et al. 2000a for a review).

Zamanov & Marziani 2002; Marziani et al. 2001), because of the great progress in the calibration of the $R_{\text{BLR}} - L$ relationship (e.g, Kaspi et al. 2000, 2005, 2007; McLure & Jarvis 2004; Vestergaard & Peterson 2006; Peterson et al. 2004; Bentz et al. 2006) due to the recent great advance in the reverberation mapping (e.g., Kapsi et al. 2000; Peterson & Bentz 2006). We refer the reads to McGill et al. (2008, and references therein) for a summary of the existing formula used to calculate M_{BH} basing upon “single-epoch” observation. In this work, the black hole mass is estimated by the width and luminosity of $\text{H}\beta_b$ in individual object, according to the scaling law obtained by Greene & Ho (2005).

$$M_{\text{BH}} = 3.6 \times 10^6 \left(\frac{L_{\text{H}\beta}}{10^{42} \text{ erg s}^{-1}} \right)^{0.56} \left(\frac{\text{FWHM}_{\text{H}\beta}}{1000 \text{ km s}^{-1}} \right)^2 M_{\odot} \quad (3)$$

For each object, the estimated M_{BH} and L/L_{Edd} is listed in Column (10) and (11) in Table 2, respectively. The bolometric luminosity L_{bol} is estimated from the $\text{H}\beta_b$ component as described above.

The calculations of both L_{bol} and L/L_{Edd} allow us to find that the current sample is strongly biased against sub-luminous AGNs usually with low L/L_{Edd} . In fact, the left panel of Figure 4 shows the lack of AGNs with $L_{\text{bol}} < 10^{43} \text{ ergs s}^{-1}$. Figure 5 displays the distributions of the L/L_{Edd} (*left panel*) and M_{BH} (*middle panel*) for the total 42 AGNs. As shown in the middle panel, the M_{BH} is sampled within a wide range (~ 3 dex) from $10^6 M_{\odot}$ to $10^9 M_{\odot}$ with a peak at $10^{7-8} M_{\odot}$. In contrast, the left panel shows that L/L_{Edd} distributes in a relatively narrow range as compared with the previous studies. The total range of our L/L_{Edd} spans from 0.01 to 1. In particular, about $\sim 60\%$ objects listed in the sample have L/L_{Edd} between 0.01 and 0.1. However, the L/L_{Edd} of bright local AGNs usually spans at least three orders of magnitude from 1 to 0.001 (e.g., Woo & Urry 2002; Boroson 2002). Basing upon the 2-10keV X-ray luminosity, Panessa et al. (2006) indicated that the L/L_{Edd} of the Palomar optically selected AGNs ranges from 10^{-5} to 0.1. As an additional test, the right panel of Figure 4 shows the M_{BH} vs. $L_{3-20\text{keV}}$ plot. $L_{3-20\text{keV}}$ as a function of M_{BH} is over-plotted as dashed lines for three different L/L_{Edd} (i.e., 1, 0.1, and 0.01). As shown in the plot, a majority of our objects are located below the line with $L/L_{\text{Edd}} = 0.1$ and above the line with $L/L_{\text{Edd}} = 0.01$.

In summary, the hard X-ray selected AGNs listed in our sample are luminous AGNs with a wide range of M_{BH} but a nearly constant accretion activity (i.e., L/L_{Edd}), which is likely due to the selection effect of the survey that is biased toward X-ray luminous objects. In active (or luminous) AGN, the optical/UV ionizing radiation is believed to be emitted from a standard geometric thin disk (e.g., Shakura & Sunyaev 1973). The low energy photon is comptonized by a hot corona to produce the hard X-ray emission below 10keV (Haardt & Maraschi 1991). A Compton recoil of the soft photon is required to occur on the ionized

surface of the accretion disk to produce the emission spectrum beyond 10keV. The main observation feature of the reflection is a bump peaked at about 30keV (e.g., George & Fabian 1991; Zycki et al. 1994; Ross & Fabian 2002, 2005).

The bias towards active AGNs could be possibly caused by the fact that either intensive Compton reflection takes place only in AGNs at high state with large L/L_{Edd} or the surveys are biased against the Compton-thick objects. In the first case, the theory of the Compton reflection predicts that the X-ray emission contributed by the reflection depends primarily on the X-ray ionizing parameter, and secondarily on the UV radiation produced by the dissipation inside the accretion disk. In the second case, our analysis implies a possible connection between the less X-ray absorption and high L/L_{Edd} in broad-line AGNs. In fact, we selected the objects with regardless of their X-ray spectral properties. Figure 1 shows the lack of objects with large column density in the sample. We believe that the sample completeness would be improved by including the ongoing *Swift*/BAT survey with large effective collecting area and harder energy bandpass (14-195 keV) in the future studies.

Figure 4 shows that the hard X-ray luminosity is strongly correlated with the M_{BH} in our sample. In fact, the correlation is naturally expected given the tight $L_{3-20\text{keV}}$ vs. L_{bol} correlation and nearly constant L/L_{Edd} . The L_X vs. M_{BH} correlation provides us a potential estimate of black hole mass for luminous AGNs within $0.01 \leq L/L_{\text{Edd}} \leq 0.1$. The following relationship is obtained by us through a least square fitting: $\log(M_{\text{BH}}/M_{\odot}) = (0.82 \pm 0.09) \log L_{3-20\text{keV}} - (28.23 \pm 3.78)$. Our results conflicts with Panessa et al. (2006) and Pellegrini (2005) who did not find the correlation, but is in agreement with Kiuchi et al. (2006). Panessa et al. (2006) investigated a sample of 47 nearby Seyfert galaxies selected from the Palomar spectroscopy (Ho et al. 1997). The luminosity obtained by different X-ray instruments is down to $L_{2-10\text{keV}} \sim 10^{38} \text{ergs s}^{-1}$. The studies in Pellegrini (2005) are based on the *Chandra* observations down to a luminosity $L_{2-10\text{keV}} \sim 10^{38} \text{ergs s}^{-1}$. Kiuchi et al. (2006) used the broad-line AGN sample detected by the *ASCA* Large Sky Survey (ALSS) and *ASCA* Medium Sensitivity Survey in the northern sky (AMSSn) with a detection limit of a few $\times 10^{-13} \text{ ergs s}^{-1} \text{ cm}^{-2}$ in 2-10keV bandpass. As discussed above, it is worthy noting that the correlation most likely does not reflect the physics but a selection effect of the surveys.

5.3. Fe II ratio vs. disk temperature relation

As a key parameter in the EI space, the Fe II ratio (RFe) is defined as the ratio of the optical Fe II complex to $\text{H}\beta$. Although the total Fe II emission increases by fourfold with reasonable ionization parameter in AGN (Korista et al. 1997), traditional photoionization

models can not explain the strong Fe II emission in optical and UV bands (e.g, Netzer & Wills 1983; Joly 1987; Collin-Souffrin et al. 1988). At present, the problem is only slightly alleviated by the major improvements in the atomic data and by the improved treatment of the line excitation process (Sigut & Pradhan 2003; Baldwin et al. 2004). We refer the reads to Collin & Joly (2000) for a summary of the mechanisms that can enhance the Fe II emission. BG92 put forward a picture in which the RFe is determined by the vertical structure of the accretion disk. The vertical structure is governed by L/L_{Edd} . A large L/L_{Edd} leads to a large X-ray heated volume that could generate large Fe II emission. Sulentic et al. (2000b) developed a semi-analysis model in which the RFe depends on L/L_{Edd} as $\text{RFe} \propto 0.55 \log(L/L_{\text{Edd}})$. Although the RFe is found to generally increase with L/L_{Edd} in optical bright quasars, Netzer et al. (2004) found that a number of high- z quasars deviate the trend, i.e., with very small RFe but large L/L_{Edd} (see also in Netzer & Trakhtenbrot 2007). Using the large database provided by the Sloan Digital Sky Survey, Netzer & Trakhtenbrot (2007) recently suggested that the enhanced RFe is mainly caused by increased metal abundance.

In the current sample, the distribution of RFe is shown in the right panel of Figure 5. RFe uniformly ranges from 10^{-3} to 1. On the contrary, L/L_{Edd} distributes in a quite narrow range as describe above. In fact, no correlation between RFe and L/L_{Edd} is found in our sample (see the upper panel in Figure 6), which motivates us to suspect that RFe does not depend on L/L_{Edd} only. RFe is plotted against the characteristic disk temperature T_{max} in the bottom panel in Figure 6. The temperature scales with L/L_{Edd} and M_{BH} as predicted by the standard geometric thin disk model (e.g., Shakura & Sunyaev 1973). The exact formula of disk temperature depends on various accretion disk models. For a rapidly rotating Kerr hole, with a spin parameter $a_* = 0.998$ and efficiency of 0.31, we have $T_{\text{max}} = 10^{5.56} (L/L_{\text{Edd}})^{1/4} M_{\text{BH}}^{-1/4}$ K. The diagram indicates an obvious correlation between the two parameters. A spearman rank-order test calculated by survival analysis yields a formal correlation coefficient $r_s = 0.414$ ($P = 0.0088$, where P is the probability of null correlation). The correlation is not highly significant probably because of the small sample size. The estimated temperature spans about one order of magnitude ($\Delta \log T_{\text{max}} \approx 1.25$), corresponding to a factor of ~ 18 . The correlation then suggests a trend of more intensive Fe II emission for higher disk temperature. A marginal dependence of the continuum shape of QSOs on T_{max} was recently identified by Bonning et al. (2007) who compared the observations of SDSS with the NLTE models of accretion disk. The current result means that the strength of the Fe II emission is likely controlled by the spectral shape of the ionizing continuum.

5.4. Equivalent width of $H\beta$ vs. L_X

The physical reason of the absence of the Baldwin relationship (Baldwin 1977) for low ionization emission lines is still an open question. In fact, a weak inverse Baldwin relationship for $H\beta$ has been demonstrated by recent studies basing upon large AGN samples (e.g., Croom et al. 2002; Greene & Ho 2005). We identify a tight, positive correlation between L_X and $EW(H\beta_b)$ in our hard X-ray selected AGNs (i.e., an inverse Baldwin relationship). Figure 7 presents the correlation with correlation coefficient $r = 0.611$ ($P = 10^{-4}$) estimated by the spearman rank-order analysis. $EW(H\beta_b)$ roughly scales with hard X-ray luminosity as $EW(H\beta_b) \propto L_X^{0.39}$. Wilkes et al. (1999) identified a marginal Baldwin effect in $H\beta$ line. Noted that they examined only the luminous local quasars with $L_{1-10\text{keV}} > 10^{44}$ ergs s^{-1} .

Although many models are developed to explain the Baldwin effect for high ionization emission lines (e.g., C IV, Wandel 1999; Korista et al. 1998; Shields et al. 1995; Wills et al. 1999; Baskin & Loar 2004; Bachev et al. 2004), these models can not explain the difference between C IV and $H\beta$. Croom et al. (2002) suggested that the inverse Baldwin relationship could be explained if the longer wavelength continuum contains emission from other components (e.g., thermal dust emission, non-thermal radio emission, starlight). We estimate the possible contribution of the unknown sources as follows. We start from the relationship $\log L_X = 39.08 + 2.56 \log EW(H\beta)$, and re-write $EW(H\beta) = L(H\beta)/(L' + L_c)$, where L_c and L' is the AGN luminosity and luminosity of other unknown sources at the $H\beta$ wavelength, respectively. The X-ray luminosity could be replaced by L_c given Eq. (2) and the bolometric correction factor of 9. Replacing $L(H\beta)$ as L_c given Eq.(1) finally yields a relationship $\log(1 + L'/L_c) = 9.48 - 0.21 \log L_c$. Considering the typical case with $L_c \sim 10^{44}$ erg s^{-1} , about 40% of the observed continuum at $H\beta$ wavelength is estimated to be contributed by the unknown sources.

6. Conclusion

The properties (L/L_{Edd} and M_{BH}) of accretion onto SMBH are examined in a sample of 42 hard X-ray selected (3-60keV) broad-line AGNs in terms of their optical spectra taken by us. The energy range is harder than that usually used in the similar previous studies. These AGNs are mainly compiled from the RXTE All Sky Survey (Sazonov & Revnivtsev 2004), and are complemented by the released *INTEGRAL* AGN sample (Bassani et al. 2006a). The statistical analysis allows us to draw the following conclusions:

1. We confirm the tight correlation between the hard X-ray and optical emission line luminosities (and bolometric luminosity) in our sample, which suggests a close link

between the hard X-ray emission reflected by the ionized surface of the accretion disk and UV/optical radiation. Using the hard X-ray luminosity, a strong inverse Baldwin relationship of the $H\beta$ emission line is identified in the sample.

2. The hard X-ray selected broad-line AGNs listed in the sample are found to be strongly biased toward luminous AGNs with high L/L_{Edd} and low column density. Since L/L_{Edd} is constant (mostly between 0.01 and 0.1) in a first order approximation, the hard X-ray luminosity is strongly correlated with the black hole mass in our sample, which is most likely due to the selection effect of the surveys.
3. Although the RFe parameter is independent on L/L_{Edd} in our sample, it is found to be correlated with the accretion disk temperature as assessed by $T \propto (L/L_{\text{Edd}})M_{\text{BH}}^{-1}$. This result implies that the strength of the Fe II emission is determined by the shape of the ionizing spectrum.

Finally, it should be mentioned that a new era in AGN hard X-ray study will be opened in next a few years due to the launch of new missions with enhanced hard X-ray detection capability in not only sensitivity, but also imaging, such as Simbol-X, NeXT and NuSTAR. These missions will provide larger, and more complete samples to study the present open issues.

We would like to thank the anonymous referee for his/her valuable comments that help to improve the paper. The authors are grateful to Todd A. Boroson and Richard F. Green for providing us the Fe II template. Special thanks go to the staff at Xinglong observatory as a part of National Astronomical Observatories, China Academy of Science for their instrumental and observational help. This search is supported by the NFS of China under grant 10503005.

REFERENCES

- Antonucci, R., 1993, ARA&A, 31, 473
- Bachev, R., et al., 2004, ApJ, 617, 171
- Baldwin, J. A., 1977, ApJ, 214, 679
- Baldwin, J. A., Ferland, G. J., Korista, K. T., et al., 2004, ApJ, 615, 610
- Barthelmy, S. D., Barbier, L. M., Cummings, J. R., et al., 2005, SSRV, 120, 143

- Baskin, A., & Loar, A., 2004, MNRAS, 350, L31
- Bassani, L., Malizia, A., Stephen, J. B., et al., 2006b, arXiv: astro-ph/10455
- Bassani, L., Molina, M., Malizia, A., et al., 2006a, ApJ, 636, L65
- Beckmann, V., Gehrels, N., Shrader, C. R., et al., 2006, ApJ, 638, 642
- Bennett, C. L., Halpern, M., Hinshaw, G., et al., 2003, ApJS, 148, 1
- Bentz, M. C., Peterson, B. M., Pogge, R. W., et al., 2006, ApJ, 644, 133
- Bird, A. J., Barlow, E. J., Bassani, L., et al., 2006, ApJ, 636, 765
- Bonning, E. W., Cheng, L., Shields, G. A., et al., 2007, ApJ, 659, 211
- Boroson, T. A., 2002, ApJ, 565, 78
- Boroson, T. A., & Green, R. F., 1992, ApJS, 80, 109 (BG92)
- Brusa, M., Zamorani, G., Comastri, A., et al., 2007, ApJS, 172, 353
- Cardamone, C. N., Moran, E. C., & Kay, L. E., 2007, AJ, 134, 1264
- Cardelli, J. A., Clayton, G. C., & Mathis, J. S., 1989, ApJ, 345, 245
- Comastri, A., Setti, G., Zamorani, G., et al., 1995, A&A, 296, 1
- Collin, S., Hameury, J. M., & Joly, M., A&A, 205, 19
- Collin, S., & Joly, M., 2000, NewAR, 44, 531
- Croom, S. M., Smith, R. J., Boly, B. J., et al., 2001, MNRAS, 322, L29
- Dadina, M., 2008, astro-ph/arXiv0801.4338, accepted by A&A
- De Luca, A., & Molendi, S., 2004, A&A, 419, 837
- Dimitrijevic, M. S., Popovic, L. C., Kovacevic, L., et al., 2007, MNRAS, 374, 1181
- Elvis, M., Soltan, A., & Keel, W. C., 1984, ApJ, 283, 479
- Ferrando, P., Arnaud, M., Cordier, B., et al., 2003, arXiv:astro-ph/0309424
- Gehrels, N., Chincarini, G., Giommi, P., et al., 2004, ApJ, 611, 1005
- George, I. M., & Fabian, A. C., 1991, MNRAS, 249, 352

- Gilli, R., Comastri, A., & Hasinger, G., 2007, *A&A*, 463, 79
- Greene, J. E., & Ho, L. C., 2005, *ApJ*, 630, 122
- Grupe, D., 2004, *AJ*, 127, 1799
- Haardt, F., & Maraschi, L., 1991, *ApJ*, 1991, 380, L51
- Hasinger, G., Miyaji, T., & Schmidt, M., 2005, *A&A*, 441, 417
- Heckman, T. M., Kauffmann, G., Brinchmann, J., et al., 2005, *ApJ*, 613, 109
- Heckman, T. M., Ptak, A., Hornschemeier, A., et al., 2005, *ApJ*, 634, 161
- Ho, L. C., 2005, *Active Galactic Nuclei: From central Engine to Host Galaxy*, ASPC, Ser, 290, 379
- Ho, L. C., Filippenko, A. V., & Sargent, W. L., 1997, *ApJS*, 112, 315
- Hu, C., Wang, J. M., Ho, L. C., et al., 2008, astro-ph/arXiv:0807.2060, accepted by *ApJL*
- Joly, M., 1987, *A&A*, 184, 33
- Kaspi, S., Smith, P. S., Netzer, H., et al., 2000, *ApJ*, 533, 631
- Kaspi, S., Smith, P. S., Netzer, H., et al., 2005, *ApJ*, 629, 61
- Kaspi, S., Brandt, W. N., Maoz, D., et al., 2007, *ApJ*, 659, 997
- Kauffmann, G., Heckman, T. M., Tremonti, C., et al., 2003, *MNRAS*, 346, 1055
- Kawaguchi, T., Shimura, T. & Mineshige, S., 2001, *ApJ*, 546, 966
- Kiuchi, G., Ohta, K., Akiyama, M., et al., 2006, *ApJ*, 647, 892
- Korista, K., Baldwin, J., & Ferland, G., 1998, *ApJ*, 507, 24
- Korista, K., Baldwin, J., Ferland, G., et al., 1997, *ApJS*, 108, 401
- Kriss, G., 1994, *Adass*, 3, 437
- Krivonos, R., Revnivtsev, M., Lutovinov, A., et al., 2007, *A&A*, 475, 775
- Levenson, N. A., Heckman, T. M., Krolik, J. H., et al., 2006, 648, 111
- Lira, P., Ward, M. J., Zezas, A., et al., 2002, *MNRAS*, 333, 709

- Lira, P.; Ward, M. J., Zezas, A., et al., 2002, MNRAS, 330, 259
- Markwardt, C. B., Tuller, J., Skinner, G. K., et al., 2005, ApJ, 633, L77
- Marziani, P., Sulentic, J. W., Zamanov, R., et al., 2003, MmsAI, 74, 490
- Marziani, P., Sulentic, J. W., Zwitter, T., et al., 2001, ApJ, 558, 533
- Masetti, N., Palazzi, E., Bassani, L., et al., 2004, A&A, 426, L41
- Massey, P., Strobel, K., Barnes, J. V., et al., 1988, ApJ, 328, 315
- McGill, K. L., Woo, J., Treu, T., et al., 2008, ApJ, 673, 703
- McLure, R. J., & Jarvis, M. J., 2004, MNRAS, 353, L45
- Moran, E. C., Filippenko, A. V., & Chornock, R., 2002, ApJ, 579, L71
- Mulchaey, J. S., Koratkar, A., Ward, M. J., et al., 1994, ApJ, 436, 586
- Mullaney, J. R., & Ward, M. J., 2008, MNRAS, 385, 53
- Netzer, H., Mainieri, V., Rosati, P., et al., 2006, A&A, 453, 525
- Netzer, H., Shemmer, O., Maiolino, R., et al., 2004, ApJ, 614, 558
- Netzer, H., & Trakhtenbrot, B., 2007, ApJ, 654, 754
- Netzer, H., & Wills, B. J., 1983, ApJ, 275, 445
- O’Sullivan, E., Forbes, D. A., & Ponman, T. J., 2001, MNRAS, 328, 461
- Panessa, F., Bassani, L., Cappi, M., et al., 2006, A&A, 455, 173
- Panessa, F., Bassani, L., De Rosa, A., et al., 2008, A&A, 483, 151
- Piconcelli, E., Jimenez-Bailon, E., Guainazzi, M., et al., 2005, A&A, 423, 15
- Pellegrini, S., 2005, ApJ, 624, 155
- Peterson, B. M., Ferrarese, L., Gilbert, K. M., et al., 2004, ApJ, 613, 682
- Peterson, B. M., & Bentz, M. C., 2006, NewAR, 50, 796
- Reeves, J. N., & Turner, M. J. L., 2000, MNRAS, 316, 234
- Revnivtsev, M., Sazonov, S., Jahoda, K., et al., 2004, A&A, 418, 927

- Ross, R. R., & Fabian, A. C., 2002, MNRAS, 336, 315
- Ross, R. R., & Fabian, A. C., 2005, MNRAS, 358, 211
- Shakura, N. I., & Sunyaev, R. A., 1973, A&A, 24, 337
- Sazonov, S. Y., & Revnivtsev, M. G., 2004, A&A, 423, 469
- Sazonov, S., Revnivtsev, M., Krivonos, R., et al., 2007, A&A, 462, 57
- Severgnini, P., Caccianiga, A., Braitto, V., et al., 2003, A&A, 406, 483
- Shields, J. C., Ferland, G. J., & Peterson, B. M., 1995, ApJ, 411, 507
- Sigut, T. A. A., & Pradhan, A. K., 2003, ApJS, 145, 15
- Silverman, J. D., Green, P. J., Barkhouse, W. A., et al., 2005, ApJ, 618, 123
- Sulentic, J. W., Bachev, R., Marziani, P., et al., 2007, ApJ, 666, 757
- Sulentic, J. W., Marziani, P., & Dultzin-Hacyan, D., 2000a, ARA&A, 38, 521
- Sulentic, J. W., Marziani, P., & Zwitter, T., et al., 2000b, ApJ, 545, L15
- Sulentic, J. W., Repetto, P., Stirpe, G. M., et al., 2006, A&A, 456, 929
- Takahashi, T., Kelley, R., Mitsuda, K., et al., 2008, astro-ph/arXiv:0807.2007
- Tueller, J., Mushotzky, R. F., Barthelmy, S., et al., 2008, ApJ, 681, 113
- Ubertini, P., Lebrun, F., Di Cocco, G., et al., 2003, A&A, 411, L131
- Veron-Cetty, M.-P., & Veron, P., 2006, A&A, 455, 773
- Veron-Cetty, M.-P., Veron, P., Joly, M., et al., 2007, A&A, 475, 487
- Vestergaard, M., & Peterson, B. M., 2006, ApJ, 641, 689
- Wandel, A., 1999, ApJ, 527, 649
- Wang, J., Wei, J. Y., & He, X. T., 2005, NewA, 10, 353
- Wang, J., Wei, J. Y., & He, X. T., 2006, ApJ, 638, 106
- Wang, J., & Wei, J. Y., 2008, ApJ, 679, 86
- Wang, T., Brinkmann, W., & Bergeron, J., 1996, A&A, 309, 81

- Ward, M. J., Done, C., Fabian, A. C., et al., 1988, *ApJ*, 324, 767
- Wilkes, B. J., Kuraszekiewicz, J., Green, P. J., et al., 1999, *ApJ*, 513, 76
- Wills, B. J., Bortherton, M. S., Fang, D., et al., 1993, *ApJ*, 415, 563
- Winkler, C., Courvoisier, T. J. -L., Di Cocco, G., et al., 2003, *A&A*, 411, L1
- Worsley, M. A., Fabian, A. C., Bauer, F. E., et al., 2005, *MNRAS*, 357, 1281
- Xu, D. W., Komossa, S., Wei, J. Y., et al., 2003, *ApJ*, 590, 73
- Zamanov, R., & Marziani, P., 2002, *ApJ*, 571, L77
- Zdziarski, A. A., Johnson, W. N., & Done, C., et al., 1995, *ApJ*, 438, L63
- Zdziarski, A. A., Poutanen, J., & Johnson, W. N., 2000, *ApJ*, 542, 703
- Zezas, A., Hernquist, L., Fabbiano, G., et al., 2003, *ApJ*, 699, L73
- Zycki, P. T., Krolik, J. H., Zdziarski, A. A., et al., 1994, *ApJ*, 437, 597

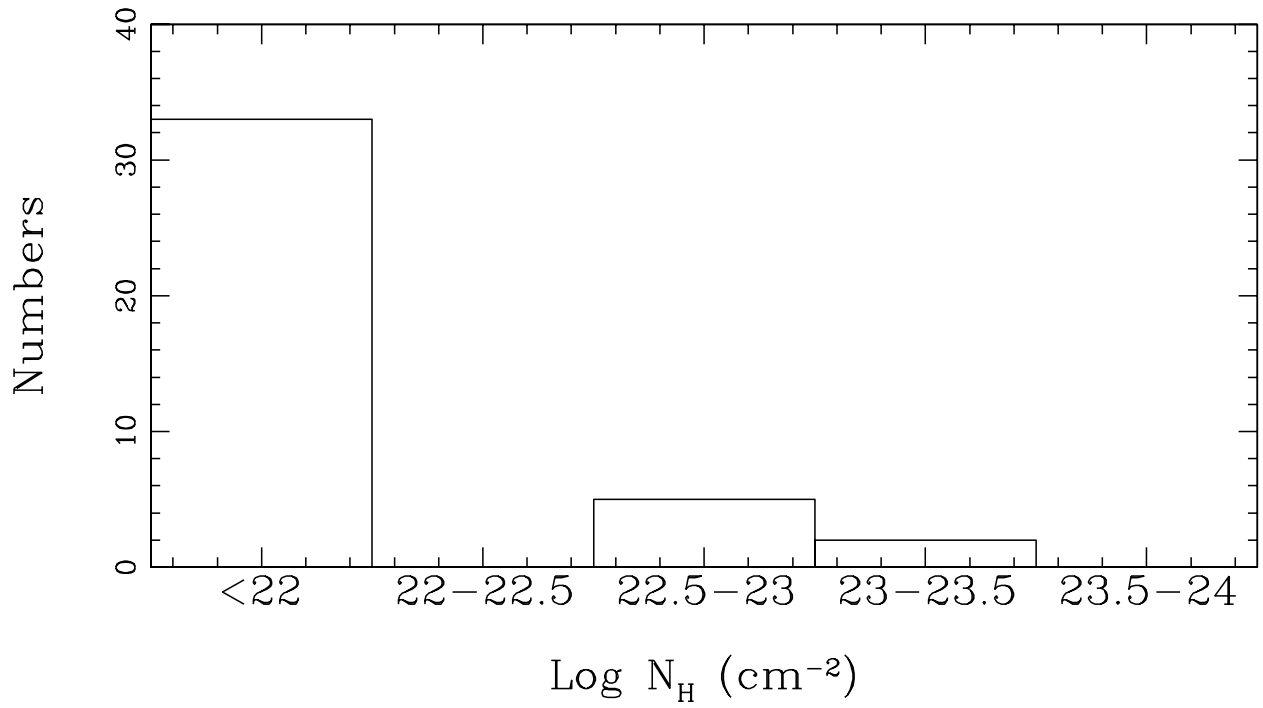


Fig. 1.— Observed X-ray absorption distribution of the 42 hard X-ray selected broad-line AGNs listed in the sample.

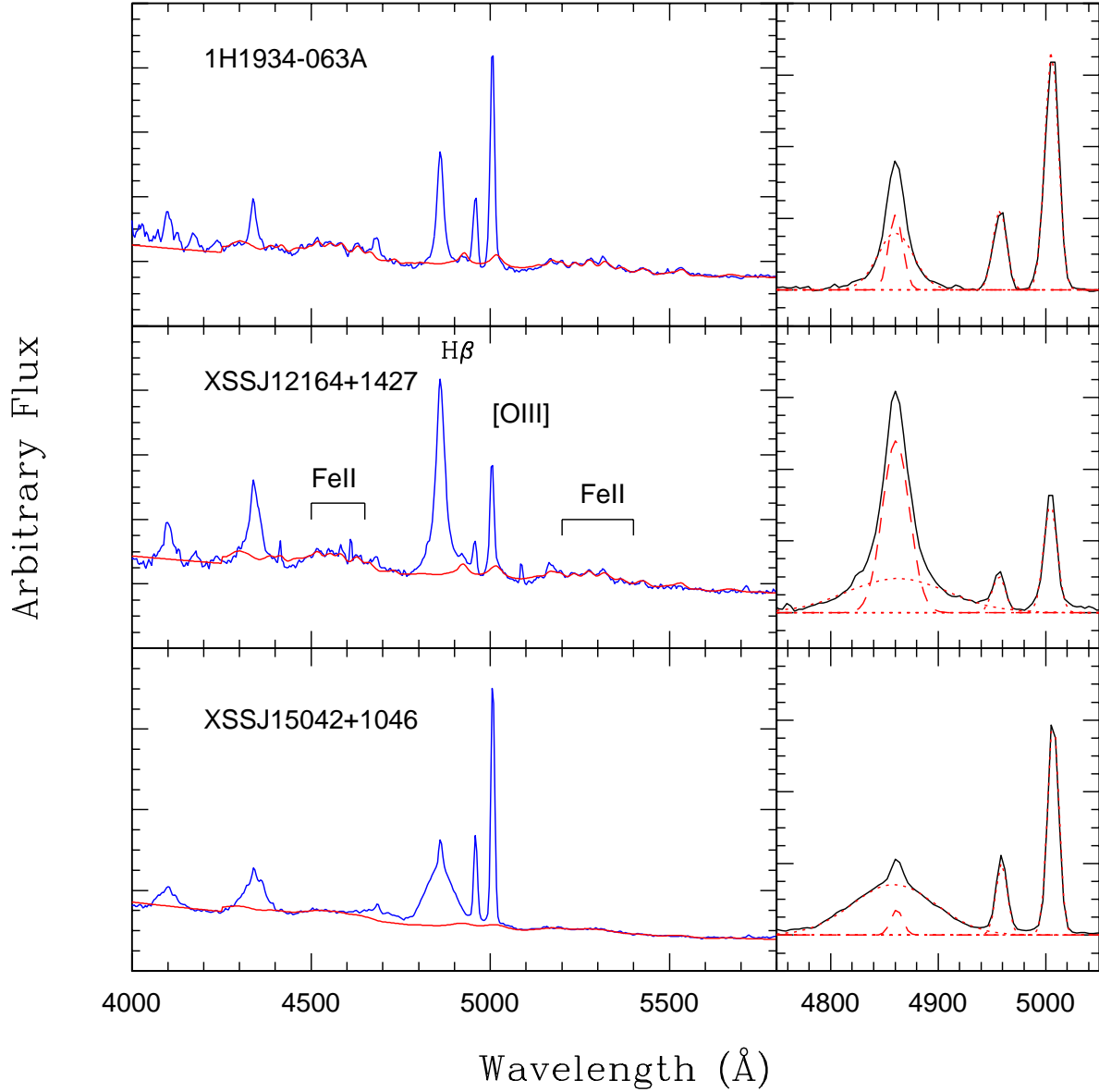


Fig. 2.— *left column*: the modeling of the continuum and Fe II complex around H β region for three typical cases. In each panel, the blue curve shows the observed spectrum, and the overlaid red one the modeled spectrum (continuum + Fe II complex). The strong emission lines, especially the two strong Fe II complex around the H β , are marked on the figure. *right column*: the modeling of the emission-line profile by a set of Gaussian components for the H β and [O III] doublet in the three cases, after subtract the modeled continuum and Fe II complex. In each panel, the observed profile is shown by the black curve. The three red short dashed lines show the modeled H β broad component and [O III] doublet. The modeled narrow H β emission is presented by the long dashed line.

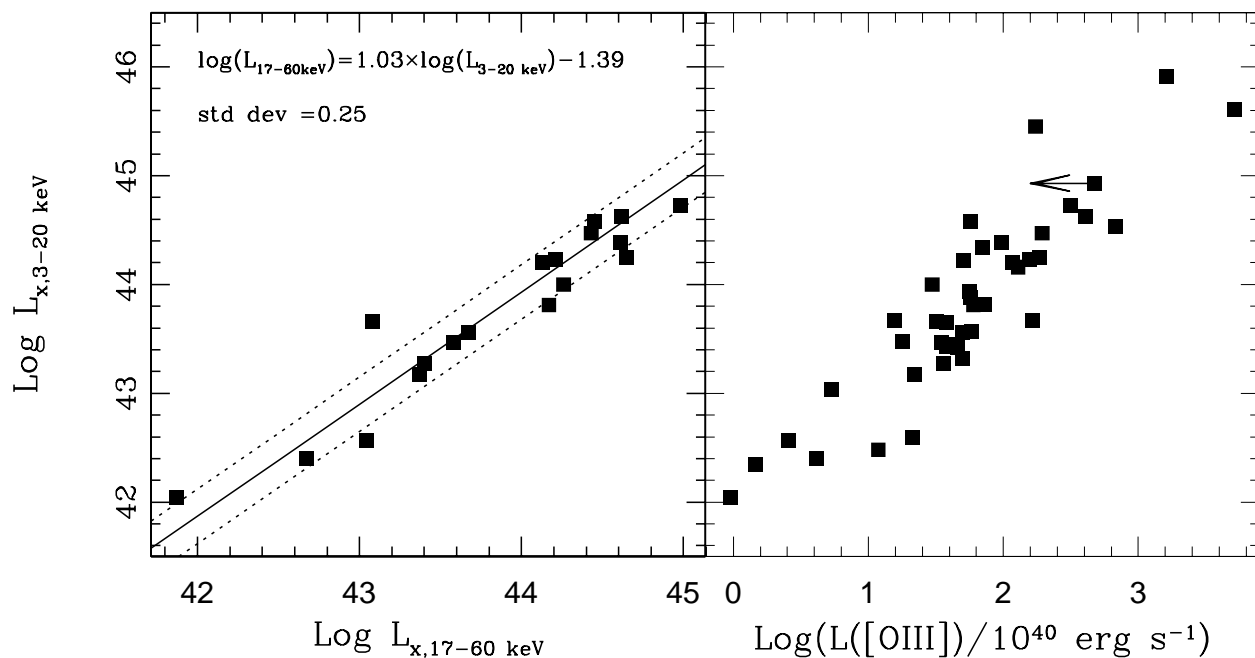


Fig. 3.— *left panel:* the luminosity in the energy bandpass 3-20 keV plotted against the luminosity in 17-60 keV for the 18 objects detected by both XSS and *INTEGRAL*. The solid line shows the best fit to the data without taking into account of the errors. The 1σ dispersion is marked by the two dashed lines. *right panel:* the tight correlation between the [O III] emission line and 3-20 keV luminosity.

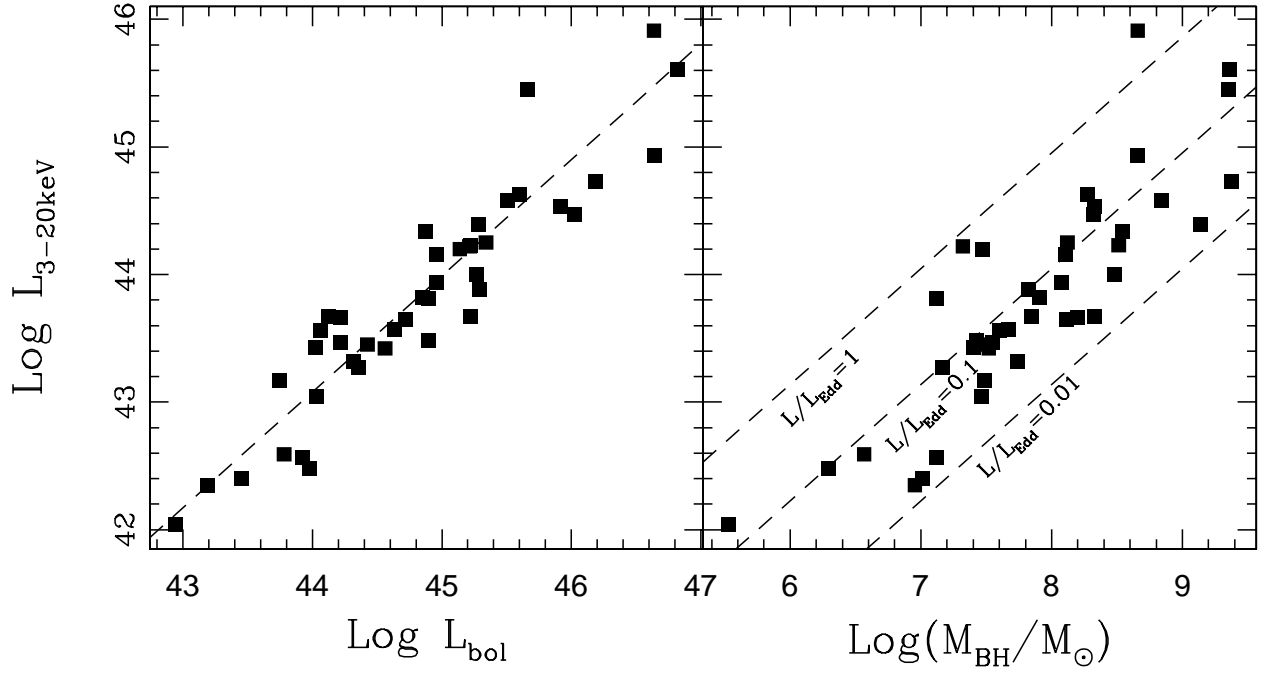


Fig. 4.— *left panel:* $L_{3-20\text{keV}}$ plotted against the bolometric luminosity estimated from the $\text{H}\beta$ broad component. The solid line shows the best fit to the data: $\log L_X = (0.91 \pm 0.06) \log L_{\text{bol}} + (3.04 \pm 2.78)$. *right panel:* Distribution on the plot of L_X vs. black hole mass. The three dashed lines show the L_X as a function of the black hole mass for different $L/L_{\text{Edd}} = 0.01, 0.1$, and 1.

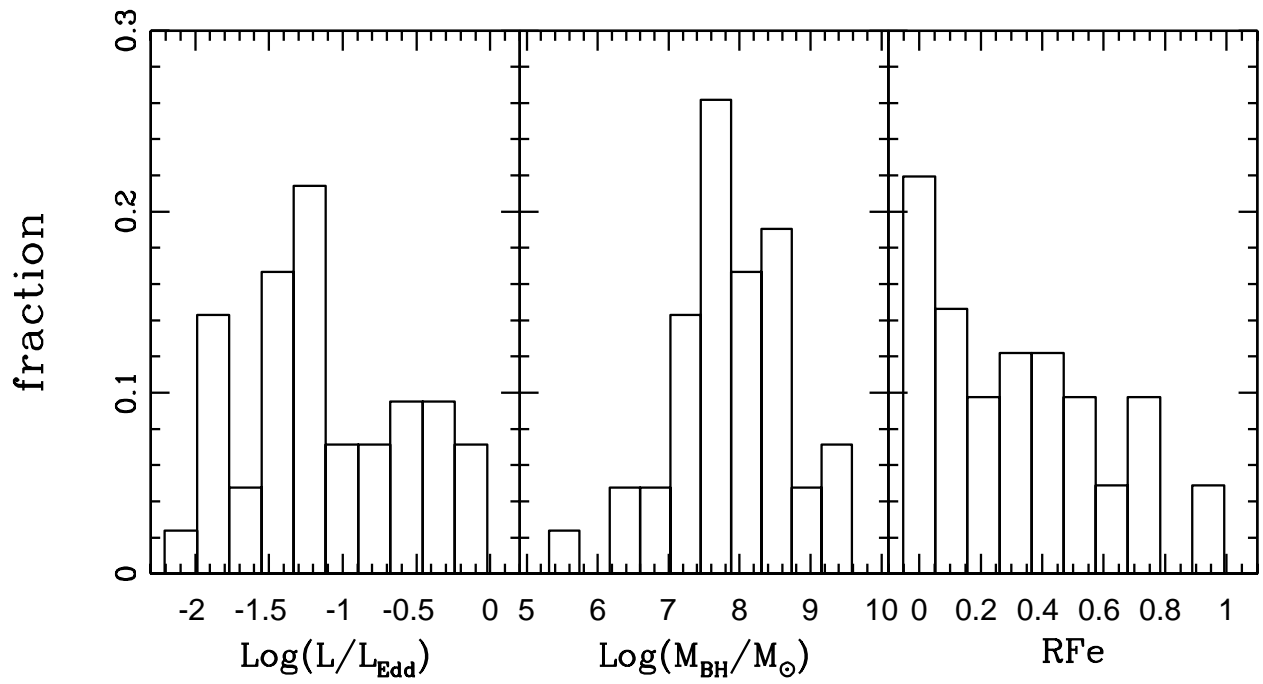


Fig. 5.— Distribution of the Eddington ratio (*left panel*), black hole mass (*middle panel*), and parameter RFe (*right panel*).

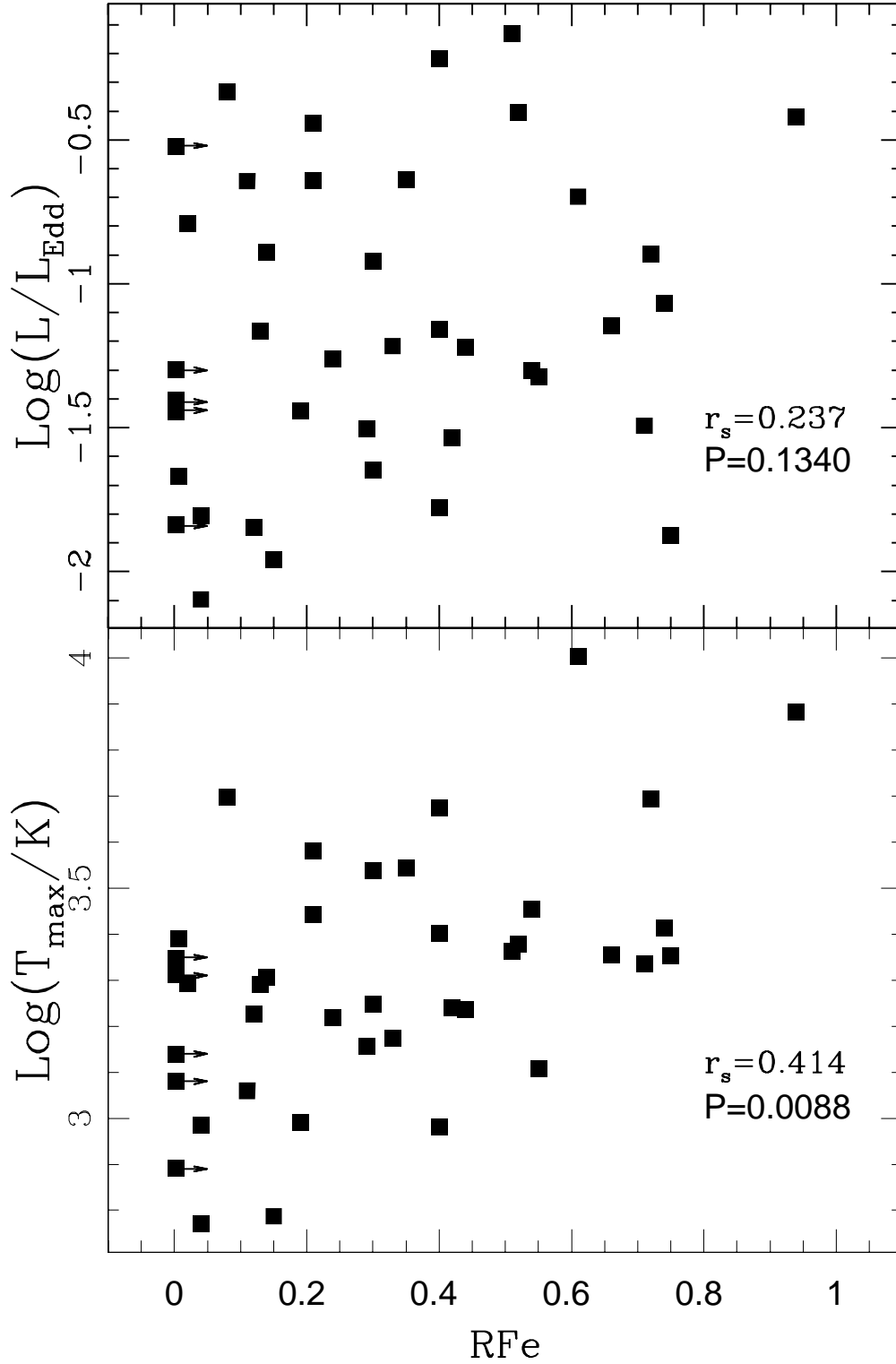


Fig. 6.— *top panel:* RFe plotted against L/L_{Edd} ($r_s = 0.237$, $P = 0.134$). *bottom panel:* the same as the top panel, but for $T_{\text{max}} = 10^{5.56}(L/L_{\text{Edd}})^{1/4}M_{\text{BH}}^{-1/4}$. The diagram shows a relatively strong correlation between the two parameters ($r_s = 0.414$, $P = 0.0088$). In both panels, the points with zero flux of the Fe II emission are indicated by superposed arrows. The correlation coefficients are calculated by survival analysis.

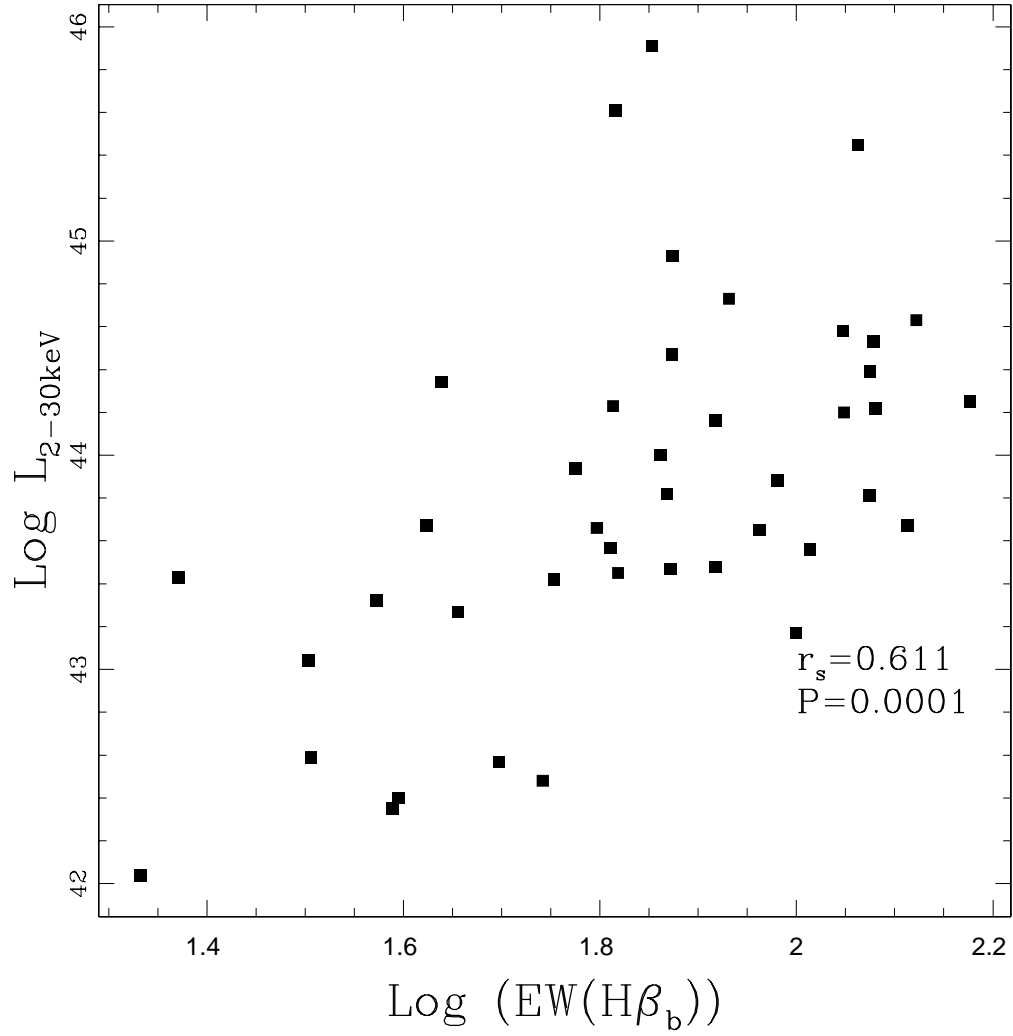


Fig. 7.— Hard X-ray luminosity is plotted as a function of equivalent width of the H β broad component. A spearman rank-order test yields a correlation coefficient $r = 0.611$ ($P = 10^{-4}$).

Table 1: Log of spectroscopic observation

Name	Other name	R.A.	Decl.	z	Date	Exposure (s)	m_v	AGN Type
(1)	(2)	(3)	(4)	(5)	(6)	(7)	(8)	(9)
XSS J00368+4557	CGCG 535-012	00 36 21.0	45 39 54	0.048	2400	2006 Aug 15	15.45	S1
QSO 0241+622	02 44 57.7	62 28 07	0.044	3600	2006 Dec 17	16.1	S1
3C 111	04 18 21.3	38 01 36	0.0485	3600	2007 Nov 03	18.0	S1
XSS J04331+0520	3C 120	04 33 11.1	05 21 16	0.033	1800	2007 Feb 16	14.2	BLRG
XSS J05103+1640	IRAS 05078+1626	05 10 45.5	16 29 56	0.018	1800	2007 Feb 16	15.6	S1
XSS J05162-0008	AKN 120	05 16 11.4	-00 08 59	0.033	1200	2006 Nov 18	14.1	S1
XSS J05552+4617	MCG +8-11-11	05 54 53.6	46 26 22	0.02	1800	2007 Feb 17	15.0	S1
Mark 6	06 52 12.2	74 25 37	0.01881	3600	2007 Feb 16	15.0	S1.5
XSS J07434+4945	MRK 79	07 42 32.8	49 48 35	0.022	1800	2005 Nov 29	14.9	S1
XSS J08117+7600	PG 0804+761	08 10 58.6	76 02 42	0.1	2400	2007 Nov 16	15.15	S1
XSS J09204+1608	MRK 704	09 18 26.0	16 18 19	0.029	1800	2006 Nov 17	15.38	S1
XSS J09261+5204	MRK 110	09 25 12.9	52 17 11	0.036	1800	2005 Nov 30	15.6	NLS1
XSS J10231+1950	NGC 3227	10 23 30.6	19 51 54	0.0038	1800	2006 Jan 31	11.1	S1
XSS J11067+7234	NGC 3516	11 06 47.5	72 34 07	0.008836	900	2006 Dec 18	12.5	S1
XSS J11417+5910	SBS 1136+594	11 39 08.9	59 11 55	0.06	2400	2007 Jan 26	15.5	S1
XSS J12032+4424	NGC 4051	12 03 09.6	44 31 53	0.0023	1200	2006 Nov 16	10.83	NLS1
XSS J12106+3927	NGC 4151	12 10 32.6	39 24 21	0.0033	1800	2006 Jan 29	11.5	S1
XSS J12164+1427	PG 1211+143	12 14 17.7	14 03 13	0.081	3600	2006 Feb 04	14.63	NLS1
NGC 4253	12 18 26.5	29 48 46	0.01293	1200	2006 Dec 21	13.7	S1.5
XSS J12206+7509	MRK 205	12 21 44.0	75 18 38	0.07	2400	2007 Jan 27	14.5	S1
XSS J12288+0200	3C 273	12 29 06.7	02 03 08	0.15834	900	2006 Dec 21	12.86	RLQ
XSS J12408-0516	NGC 4593	12 39 39.4	-05 20 39	0.009	1200	2007 Jan 26	14.67	S1
XSS J13420-1432	NPM1G-14.0512	13 41 12.9	-14 38 41	0.042	2400	2008 Mar 13	15.50	NLS1
XSS J13530+6916	MRK 279	13 53 03.4	69 18 30	0.031	1200	2007 Feb 16	14.57	S1
XSS J14181+2514	NGC 5548	14 17 59.5	25 08 12	0.017	1800	2008 Mar 03	13.3	S1
XSS J15042+1046	MRK 841	15 04 01.2	10 26 16	0.036	1200	2007 Feb 16	14.0	S1
XSS J15348+5750	MRK 290	15 35 52.3	57 54 09	0.030	2400	2008 Mar 13	15.1	S1
XSS J17276-1359	PDS 456	17 28 19.8	-14 15 56	0.184	1800	2007 Sep 07	14.69	RQQ
XSS J17413+1851	4C +18.51	17 42 07.0	18 27 21	0.19	2400	2007 Sep 07	16.43	RLQ
XSS J18196+6454	H 1821+643	18 21 57.3	64 20 36	0.297	1800	2006 Aug 16	14.1	RQQ
XSS J18348+3238	3C 382	18 35 02.1	32 41 50	0.059	1800	2006 Aug 16	15.5	BLRG
XSS J18408+7947	3C 390.3	18 42 09.0	79 46 17	0.056	1800	2006 Aug 15	14.37	BLRG
1H 1934-063A	19 37 33.0	-06 13 05	0.01059	1800	2006 Aug 16	14.09	S1
NGC 6814	19 42 40.6	-10 19 25	0.00521	1800	2007 Nov 04	12.06	S1.5
XSS J20404+7521	4C +74.26	20 42 37.3	75 08 02	0.1	1800	2006 Sep 15	15.13	RLQ
XSS J20441-1042	MRK 509	20 44 09.7	-10 43 25	0.034	1800	2006 Sep 15	13.0	S1
XSS J21128+8216	S5 2116+81	21 14 01.2	82 04 48	0.084	2400	2006 Aug 15	15.7	BLRG
XSS J22423+2958	AKN 564	22 42 39.3	29 43 31	0.025	1800	2006 Nov 15	14.55	NLS1
XSS J22539-1735	MR 2251-178	22 54 05.8	-17 34 55	0.064	1800	2006 Nov 15	14.36	RQQ
XSS J23033+0858	NGC 7469	23 03 15.6	08 52 26	0.016	1800	2006 Aug 15	13.0	S1
XSS J23040-0834	MRK 926	23 04 43.5	-08 41 09	0.047	1800	2007 Nov 03	14.6	S1
XSS J23073+0447	PG 2304+042	23 07 02.9	04 32 57	0.042	2400	2007 Nov 02	15.44	S1

Table 2. List of properties of the hard X-ray selected AGNs

Name	EW($H\beta_n$) Å	EW($H\beta_b$) Å	RFe	$\log[L(H\beta_b)]$ ergs s ⁻¹	FWHM($H\beta_b$) km s ⁻¹	$\log[L([OIII])]$ ergs s ⁻¹	$\log[L_{2-30\text{keV}}]$ ergs s ⁻¹	$\log[L_{17-60\text{keV}}]$ ergs s ⁻¹	$\log(M_{\text{BH}}/M_{\odot})$	L/L_{Edd}
(1)	(2)	(3)	(4)	(5)	(6)	(7)	(8)	(9)	(10)	(11)
XSSJ 00368+4557	82.6	0.35	42.1	2555	41.3	43.48	7.42	0.23
QSO 0241+622	43.6	0.26	42.1	9401	41.8	44.34	44.28	8.54	0.02
3C 111	119.9	0.00	43.3	3445	42.8	44.53	44.59	8.33	0.30
XSS J04331+0520	10.5	82.7	0.24	42.2	5367	42.1	44.16	8.11	0.06
XSS J05103+1640	9.0	74.5	> 0.	41.3	4855	41.5	43.47	43.58	7.55	0.04
XSS J05162-0008	2.3	72.7	0.55	42.5	6595	41.5	44.	44.26	8.48	0.05
XSS J05552+4617	53.5	103.2	0.30	41.2	5761	41.7	43.56	43.67	7.60	0.02
Mark 6	6.0	37.4	0.42	41.4	5627	41.7	43.32	43.41	7.74	0.03
XSS J07434+4945	8.6	65.8	0.40	41.6	3815	41.7	43.45	7.47	0.07
XSS J08117+7600	74.7	0.52	43.4	3146	42.3	44.47	44.43	8.32	0.39
XSS J09204+1608	6.9	91.8	0.29	41.9	6421	41.6	43.65	8.11	0.03
XSS J09261+5204	118.6	0.08	42.1	1798	41.8	43.81	44.17	7.12	0.47 ¹
XSS J10231+1950	5.1	39.3	0.007	40.5	4556	40.6	42.4	42.67	7.01	0.04 ²
XSS J11067+7234	31.9	41.1	5020	40.7	43.04	7.46	0.03 ₁
XSS J11417+5910	7.3	73.8	0.13	42.0	4608	41.9	43.82	7.91	0.07
XSS J12032+4424	21.5	0.61	39.9	1202	40.0	42.04	41.87	5.53	0.20
XSS J12106+3927	37.2	100.0	0.12	40.8	6354	41.3	43.17	43.37	7.49	0.01
XSS J12164+1427	120.3	0.40	42.5	1804	41.7	44.22	7.32	0.60
NGC 4253	11.3	32.1	0.72	40.8	2153	41.3	42.59	42.7	6.57	0.13
XSS J12206+7509	95.6	0.21	42.5	3037	41.8	43.88	7.83	0.23
XSS J12288+0200	71.3	0.51	44.1	2970	43.2	45.91	45.92	8.66	0.74
XSS J12408-0516	49.8	0.54	41.0	3654	40.4	42.57	43.04	7.12	0.05
XSS J13420-1432	15.3	64.6	0.66	41.8	4112	41.8	43.57	7.67	0.07
XSS J13530+6916	5.7	59.6	0.44	42.2	5147	41.8	43.94	8.07	0.06
XSS J14181+2514	7.8	62.7	0.04	41.3	10312	41.5	43.66	43.08	8.20	0.008
XSS J15042+1046	9.4	129.6	0.33	42.5	5709	42.2	43.67	8.33	0.061
XSS J15348+5750	4.2	23.5	0.71	41.1	4740	41.6	43.43	7.41	0.03
XSS J17276-1359	74.6	3.58	44.1	2957	< 42.7	44.93	8.66	0.75
XSS J17413+1851	1.8	115.5	0.04	43.0	13506	42.2	45.45	9.35	0.02
XSS J18196+6454	2.9	65.4	0.18	44.3	5797	43.7	45.61	9.36	0.23
XSS J18348+3238	111.4	0.19	42.8	8340	41.8	44.58	44.45	8.84	0.04
XSS J18408+7947	3.2	118.8	0.15	42.5	13799	42.0	44.39	44.61	9.13	0.01

Table 2—Continued

Name	EW($H\beta_n$) Å	EW($H\beta_b$) Å	RFe	$\log[L(H\beta_b)]$ ergs s ⁻¹	FWHM($H\beta_b$) km s ⁻¹	$\log[L([OIII])]$ ergs s ⁻¹	$\log[L_{2-30\text{keV}}]$ ergs s ⁻¹	$\log[L_{17-60\text{keV}}]$ ergs s ⁻¹	$\log(M_{\text{BH}}/M_{\odot})$	L/L_{Edd}
(1)	(2)	(3)	(4)	(5)	(6)	(7)	(8)	(9)	(10)	(11)
1H 1934-063A	55.2	0.94	41.1	1354	41.0	42.48	42.59	6.29	0.38
NGC 6814	38.8	0.75	40.2	5182	40.2	42.35	42.47	6.95	0.01
XSS J20404+7521	85.4	> 0.	43.6	9418	42.5	44.73	44.98	9.37	0.05
XSS J20441-1042	10.7	111.8	0.21	42.4	2261	42.1	44.2	44.13	7.47	0.36
XSS J21128+8216	6.3	150.0	0.14	42.6	4123	42.3	44.25	44.65	8.12	0.13
XSS J22423+2958	56.6	0.74	41.7	3649	41.7	43.42	7.52	0.09
XSS J22539-1735	5.7	132.5	0.02	42.9	4093	42.6	44.63	44.62	8.28	0.16
XSS J23033+0858	13.7	45.3	0.30	41.5	2819	41.6	43.27	43.40	7.17	0.12
XSS J23040-0834	3.4	65.1	> 0.	42.5	7083	42.2	44.23	44.21	8.51	0.04
XSS J23073+0447	2.7	42.0	> 0.	41.2	7322	41.2	43.67	7.85	0.01